High-quality ultrastructural preservation using cryofixation for 3D electron microscopy of genetically labeled tissues

Tin Ki Tsang[1*], Eric A. Bushong[2*], Daniela Boassa[2], Junru Hu[2], Benedetto Romoli[3], Sebastien Phan[2], Davide Dulcis[3], Chih-Ying Su[1δ] and Mark H. Ellisman[2,4δ]

[1]Neurobiology Section, Division of Biological Sciences,
University of California, San Diego, La Jolla, CA 92093, USA

[2]National Center for Microscopy and Imaging Research, Center for Research in Biological Systems, University of California, San Diego, La Jolla, CA 92093, USA

[3]Department of Psychiatry, School of Medicine, University of California, San Diego, La Jolla, CA 92093, USA

[4]Department of Neurosciences, School of Medicine
University of California, San Diego, La Jolla, CA 92093, USA

* These authors contributed equally to this work.
δCorrespondence: mellisman@ucsd.edu (M.H.E); c8su@ucsd.edu (C.Y.S)

ABSTRACT

Electron microscopy (EM) offers unparalleled power to study cell substructures at the nanoscale. Cryofixation by high-pressure freezing offers optimal morphological preservation, as it captures cellular structures instantaneously in their near-native states. However, the applicability of cryofixation is limited by its incompatibilities with diaminobenzidine labeling using genetic EM tags and the high-contrast *en bloc* staining required for serial block-face scanning electron microscopy (SBEM). In addition, it is challenging to perform correlated light and electron microscopy (CLEM) with cryofixed samples. Consequently, these powerful methods cannot be applied to address questions requiring optimal morphological preservation and high temporal resolution. Here we developed an approach that overcomes these limitations; it enables genetically labeled, cryofixed samples to be characterized with SBEM and 3D CLEM. Our approach is broadly applicable, as demonstrated in cultured cells, *Drosophila* olfactory organ and mouse brain. This optimization exploits the potential of cryofixation, allowing quality ultrastructural preservation for diverse EM applications.

INTRODUCTION

The answers to many questions in biology lie in the ability to examine the relevant biological structures accurately at high resolution. Electron microscopy (EM) offers the unparalleled power to study cellular morphology and structure at nanoscale resolution (Leapman, 2004). Cryofixation by high-pressure freezing (hereafter referred to as cryofixation) is the optimal fixation method for samples of thicknesses up to approximately 500 μm (Dahl and Staehelin, 1989; McDonald, 1999; Moor, 1987; Shimoni et al., 1998). By rapidly freezing the samples in liquid nitrogen (-196 °C) under high pressure (~2100 bar), cryofixation immobilizes cellular structures within milliseconds and preserves them in their near-native states. In contrast, cross-linking based chemical fixation takes place at higher temperatures (≥4 °C) and depends on the infiltration of aldehyde fixatives, a process which takes seconds to minutes to complete. During chemical fixation, cellular structures may deteriorate or undergo rearrangement (Korogod et al., 2015; Steinbrecht and Müller, 1987; Szczesny et al., 1996) and enzymatic reactions can proceed (Kellenberger et al., 1992; Sabatini, 1963), potentially resulting in significant morphological artifacts.

Cryofixation is especially critical, and often necessary, for properly fixing tissues with cell walls or cuticles that are impermeable to chemical fixatives, such as samples from yeast, plant, *C. elegans*, and *Drosophila* (Ding, 1993; Doroquez et al., 2014; Kaeser et al., 1989; Kiss et al., 1990; McDonald, 2007; Müller-Reichert et al., 2003; Shanbhag et al., 1999, 2000; Winey et al., 1995). As cryofixation instantaneously halts all cellular processes, it also provides the temporal control needed to capture fleeting biological events in a dynamic process (Hess et al., 2000; Watanabe et al., 2013; Watanabe et al., 2013; Watanabe et al., 2014).

Despite the clear benefits of cryofixation, it is incompatible with diaminobenzidine (DAB) labeling reactions by genetic EM tags. For example, APEX2 (enhanced ascorbate peroxidase) is an engineered peroxidase that catalyzes DAB reaction to render target structures electron dense (Lam et al., 2015; Martell et al., 2012). Despite the successful applications of APEX2 to

three-dimensional (3D) EM (Joesch et al., 2016), there has been no demonstration that APEX2 or other genetic EM tags can be activated following cryofixation. Conventionally, cryofixation is followed by freeze-substitution (Steinbrecht and Müller, 1987), during which water in the sample is replaced by organic solvents. However, the resulting dehydrated environment is incompatible with the aqueous enzymatic reactions required for DAB labeling by genetic EM tags.

EM structures can also be genetically labeled with fluorescent markers through correlated light and electron microscopy (CLEM). Yet, performing CLEM with cryofixed samples also presents challenges. Fluorescence microscopy commonly takes place either before cryofixation (Brown et al., 2009; Kolotuev et al., 2010; McDonald, 2009) or after the sample is embedded (Kukulski et al., 2011; Nixon et al., 2009; Schwarz and Humbel, 2009). However, if the specimen is dissected from live animals, the time taken to acquire fluorescence images delays cryofixation and could cause ultrastructural deterioration. In order for fluorescence microscopy to take place after embedding, special acrylic resins need to be used (Kukulski et al., 2011; Nixon et al., 2009; Schwarz and Humbel, 2009) and only a low concentration of osmium tetroxide stain can be tolerated (De Boer et al., 2015; Watanabe et al., 2011). These constraints limit the applicability of CLEM for cryofixed samples.

Another disadvantage of cryofixation is that *en bloc* staining during freeze-substitution is often inadequate. As a result, post-staining of ultramicrotomy sections is frequently needed for cryofixed samples (Shanbhag et al., 1999, 2000; Takemura et al., 2013). However, post-staining could be labor-intensive and time-consuming, especially for volume EM (Ryan et al., 2016; Zheng et al., 2017). Critically, on-section staining is impossible for samples imaged with block-face volume EM techniques (Briggman and Bock, 2012), such as serial block-face scanning electron microscopy (SBEM) (Denk and Horstmann, 2004). A large amount of heavy metal staining is necessary for SBEM to generate sufficient back-scatter electron signal and prevent specimen charging (Deerinck et al., 2010; Kelley et al., 1973; Tapia et al., 2012). Therefore, it

remains impossible to image cryofixed samples with SBEM or other techniques that require high-contrast staining.

To overcome these limitations of cryofixation, here we present a robust approach, named the CryoChem Method (CCM), which combines key advantages of cryofixation and chemical fixation. This technique enables labeling of target structures by genetically encoded EM tags or fluorescent markers in cryofixed samples, and permits high-contrast *en bloc* heavy metal staining sufficient for SBEM. Specifically, we rehydrate cryofixed samples after freeze-substitution to make the specimen suitable for subsequent aqueous reactions and fluorescence imaging. We further show that 3D CLEM can be achieved by combining SBEM with confocal microscopy imaging of the frozen-rehydrated specimen. We successfully apply CCM to multiple biologically significant systems with distinct ultrastructural morphologies, including cultured mammalian cells, *Drosophila* olfactory organ (antenna) and mouse brain. By overcoming critical technical barriers, our method exploits the potential of cryofixation, making it compatible with genetically encoded EM tags, fluorescence imaging before resin embedding, and any EM techniques that require substantial heavy metal staining.

RESULTS

Given that a key limitation of cryofixation arises from the dehydrated state of the samples after freeze-substitution (Figure 1), it is imperative that our approach delivers a cryofixed specimen that is fully hydrated and can then be processed at higher temperatures (4 °C or room temperature) for enzymatic reactions and/or high-contrast *en bloc* heavy metal staining. It has been demonstrated that cryofixed samples can be rehydrated for immunogold labeling following cryosectioning (van Donselaar et al., 2007), but the method only yields modest EM contrast and is not compatible with genetic labeling using APEX2 nor volume EM techniques.

The CryoChem Method

To achieve the ultrastructural preservation of cryofixation and the versatility of chemical fixation, we developed a hybrid protocol which we refer to hereafter as the CryoChem Method (CCM) (Figure 1). Importantly, we devised a freeze-substitution cocktail (see below) that allows preservation of APEX2 enzymatic activity and signals from fluorescent proteins. CCM begins with high-pressure freezing of the sample, followed by freeze-substitution in an acetone solution with glutaraldehyde (0.2%), uranyl acetate (0.1%), and water (1%), to further stabilize the cryo-preserved structures at low temperatures. After freeze-substitution, the sample is rehydrated gradually on ice with a series of acetone solutions containing an increasing amount of water or 0.1M HEPES. Once completely rehydrated, the cryofixed sample is amenable for imaging with fluorescence microscopy, DAB labeling reactions using genetically encoded tags, and the high-contrast *en bloc* staining (e.g. osmium-thiocarbohydrazide-osmium and uranyl acetate) normally reserved only for chemically fixed samples. Afterwards, samples are dehydrated through a series of ethanol solutions and acetone, then infiltrated with epoxy resin and cured using standard EM procedures. These resin embedded samples may be sectioned or imaged directly with any desired EM technique (Figure 2, see *Materials and Methods* for details).

CryoChem Method offers high-quality ultrastructural preservation and sufficient *en bloc* staining for SBEM

To determine whether CCM provides high-quality ultrastructural preservation, we first tested the method in a mammalian cell line. Using transmission electron microscopy (TEM), well-preserved mitochondria and nuclear membranes were observed in the CCM-processed cells (Figure 3—figure supplement 1). Given that cryofixation is often necessary for properly fixing tissues surrounded by a barrier to chemical fixatives, we next tested CCM in a *Drosophila* olfactory organ, the antenna, which is encased in a waxy cuticle (Figure 3A). A hallmark of optimally preserved antennal tissues prepared by cryofixation is the smooth appearance of

membrane structures (Shanbhag et al., 1999, 2000; Steinbrecht, 1980; Steinbrecht and Müller, 1987). In the insect antenna, auxiliary cells extend microlamellae to surround the olfactory receptor neurons (ORNs), forming the most membrane-rich regions in the antenna. We therefore focused on this structure to evaluate the quality of morphological preservation afforded by our method. In CCM-processed antennal tissues, we found that the delicate structures of the microlamellae were well-preserved (Figure 3A and Figure 3—video supplement 1), unlike the chemically fixed counterparts in which microlamellae were distorted (Figure 3A) (Steinbrecht, 1980). Importantly, the overall ultrastructural preservation achieved through CCM resembles that obtained by standard cryofixation and freeze-substitution protocols (Shanbhag et al., 1999, 2000).

In contrast to fly antennae, which can be dissected expeditiously and frozen in the live state, certain tissues (e.g., mouse brain) are difficult to cryofix from life without tissue damage caused by anoxia or mechanical stress associated with dissection. In these cases, cryofixation can be performed after aldehyde perfusion and still produce quality morphological preservation (Sosinsky et al., 2008). To test whether CCM can improve morphological preservation of aldehyde-perfused samples, we cryofixed vibratome sections (100 μm) from an aldehyde-perfused mouse brain and processed the sample with CCM. As a control, we used standard chemical fixation procedures to process the vibratome sections of the same brain (see *Materials and Methods* for details). Compared to chemically fixed controls, the membranes of the CCM-processed samples were markedly smoother, indicating an improvement in morphological preservation (Figure 3B). This result agrees with our previous observation that cellular morphology can be markedly improved even when cryofixation is performed after aldehyde perfusion (Sosinsky et al., 2008).

Of note, we adopted a high-contrast *en bloc* staining protocol (Deerinck et al., 2010; Tapia et al., 2012; West et al., 2010; Williams et al., 2011) when processing the *Drosophila* antennae and mouse brain. An adequate level of heavy metals was incorporated into these

cryofixed samples to allow for successful imaging by SBEM (Figure 3A and 4), even without nitrogen gas injection for charge compensation (Deerinck et al., 2017) (Figure 3-- video supplement 1 and Figure 4D). This *en bloc* staining protocol is normally reserved only for chemically fixed tissues, but is now made compatible with cryofixed samples by CCM.

CryoChem Method enables DAB labeling in cryofixed samples expressing APEX2

Next we determined if DAB labeling reaction can be performed in cryofixed samples with CCM. Using CCM-processed cultured cells expressing APEX2, we observed DAB labeling in the targeted organelles (mitochondria) in the transfected cells (Figure 4A), compared to the untransfected controls (Figure 4B). We further validated this approach in CCM-processed *Drosophila* antenna; successful DAB labeling was also detected in genetically identified ORNs expressing APEX2 with X-ray microscopy (Figure 4—video supplement 1). This imaging technique facilitates the identification of the region of interest for SBEM (Figure 4C), as we and others reported previously (Bushong et al., 2015; Ng et al., 2016). Crucially, we demonstrated that an EM volume of a genetically labeled, cryofixed ORN can be acquired with SBEM, which allows for an accurate 3D reconstruction of the ORN through semi-automated segmentation (Figure 4D). Taken together, these results demonstrate that CCM can reliably generate DAB labeling by genetically encoded EM tags in cryofixed samples.

Fluorescence is well-preserved in CryoChem-processed samples

To determine whether CCM is compatible with fluorescence microscopy, we first evaluated the degree to which fluorescence level is affected after CCM processing. Using confocal microscopy, we quantified GFP fluorescence in the soma of unfixed *Drosophila* ORNs and that from CCM-processed samples after rehydration (Figure 5). Remarkably, GFP fluorescence intensities of fresh and CCM-processed ORNs are essentially indistinguishable with respect to their distributions (Figure 5A) and average levels (Figure 5B), indicating that

CCM processing has little effect on GFP fluorescence in fly ORNs. Similarly, we observed strong GFP signals in the mouse brain after the cryofixed sample was rehydrated (Figure 5—figure supplement 1A).

Next, we asked whether this observation also applies to another type of fluorescence protein. To this end, we examined tdTomato fluorescence in the mouse brain (Figure 5—figure supplement 1B). We note that tdTomato is not a variant of GFP and is instead derived from *Discosoma sp.* fluorescence protein 'DsRed' (Shaner et al., 2004). Confocal images of the CCM-processed mouse brain showed that the tdTomato fluorescence was also well-preserved (Figure 5—figure supplement 1B) and we were able to detect the co-expression of GFP and tdTomato in a subpopulation of neurons (Figure 5—figure supplement 1C). Taken together, our results indicate that CCM-processed sample can serve as a robust substrate for fluorescence imaging.

3D correlative light and electron microscopy (CLEM) in CCM-processed samples expressing fluorescent markers

Finally, we took advantage of the fact that fluorescence microscopy can now take place in a cryofixed sample before resin embedding to develop a protocol for 3D CLEM in CCM-processed specimens (Figure 6A, see *Materials and Methods* for details). The protocol first uses the core CCM steps to deliver a frozen-rehydrated sample. Subsequently, DRAQ5 DNA stain is introduced to the sample to label the nuclei, which can then serve as fiducial markers for CLEM. Next, the region containing target cells expressing fluorescent markers is imaged with confocal microscopy, during which signals from DRAQ5 and fluorescent markers are both acquired. After confocal microscopy, the sample is *en bloc* stained with multiple layers of heavy metals (Deerinck et al., 2010; Tapia et al., 2012; West et al., 2010; Williams et al., 2011), then dehydrated and embedded as in a typical CCM protocol. Subsequently, the embedded sample is imaged with X-ray microscopy. The resulting micro-computed tomography volume can be

221 registered to the confocal volume using the nuclei as fiducial markers, so that the region of
222 interest (ROI) for SBEM can be identified. After SBEM imaging, the EM volume can be
223 registered to the confocal volume in a similar fashion for 3D CLEM.

224 As a proof of principle, we performed 3D CLEM in an aldehyde-perfused, CCM-
225 processed mouse brain expressing tdTomato in a subset of neurons. To this end, we first
226 determined if DRAQ5 staining can be performed in a frozen-rehydrated specimen. Using
227 confocal microscopy, we were able to observe DRAQ5 labeling of the nuclei in a cryofixed brain
228 slice after rehydration (Figure 6B). We used the labeled nuclei as fiducial markers to register the
229 X-ray volume with the confocal data (Figure 6B) and thereby target a ROI with tdTomato-
230 expressing neurons for SBEM imaging.

231 Similarly, we were able to register the confocal volume to the SBEM volume (Figure 6C).
232 Of note, the CLEM accuracy was ensured by using the bright heterochromatin labeling by
233 DRAQ5 and their corresponding structures in EM as finer fiducial points (Figure 6C).
234 Furthermore, the fluorescent markers made it possible to identify the target cell bodies (Figure
235 6D and Figure 6—video supplement 1) and small neuronal processes (Figure 6E and Figure
236 6—video supplement 1) in the SBEM volume. Lastly, we note that with CCM, fluorescence
237 microscopy in cryofixed specimens can take place before *en bloc* EM staining. Therefore, our
238 protocol does not require special resins for embedding and permits high-contrast staining with
239 high concentrations of osmium tetroxide.

240

241 **DISCUSSION**

242 We described here a hybrid method, named CryoChem, which combines key
243 advantages of cryofixation and chemical fixation to substantially broaden the applicability of the
244 optimal fixation technique. With CCM, it is now possible to label target structures with DAB by a
245 genetically encoded EM tag, image cells expressing fluorescent markers before resin
246 embedding and deposit high-contrast *en bloc* staining in cryofixed tissues. In addition, with

CCM, one can also perform 3D CLEM in cryofixed specimens. Our method thereby provides an important alternative to conventional cryofixation and chemical fixation methods.

The modular nature of CCM (Figure 2) makes it highly versatile as researchers can modify the modules to best suit their needs. For instance, to prevent over-staining, one can replace the high-contrast *en bloc* staining step (osmium-thiocarbohydrazide-osmium and uranyl acetate) (Deerinck et al., 2010; Tapia et al., 2012; West et al., 2010; Williams et al., 2011) with a single round of osmium tetroxide staining for thin section TEM (Figures 3B, 4A and 4B) or electron tomography. In addition, CCM is essentially compatible with a wide range of reactions catalyzed by EM tags other than APEX2 (Ellisman et al., 2015). For example, the protein labeling reactions mediated by miniSOG (Shu et al., 2011) and the tetracysteine-based methods using FlAsH and ReAsH (Gaietta et al., 2002), or the non-protein biomolecule labeling reactions using Click-EM (Ngo et al., 2016) or ChromEM (Ou et al., 2017). The versatility of CCM will likely expand the breath of biological questions that can be addressed using cryofixed samples.

In addition to using EM tags, we have also developed a 3D CLEM protocol (Figure 6A) that allows optimally and rapidly preserved EM structures to be genetically labeled with fluorescent markers in CCM-processed tissues. In contrast to EM tags, fluorescent markers do not generate electron-dense products (e.g. DAB polymers) that can obscure the subcellular structures. Moreover, with multicolor CLEM, one can utilize multiple readily available genetically encoded fluorescent markers to label different target structures or cells. Using the 3D CLEM protocol, one could also pinpoint labeled subcellular structures (e.g., microtubules) or proteins (e.g., ion channels) in an EM volume with super-resolution microscopy.

The advantages of CCM makes it particularly suited for addressing biological questions that require optimal and rapid preservation of a genetically labeled structure. For example, to construct an accurate model to describe the biophysical properties of a neuron, it is essential to acquire morphological measurements based on faithfully preserved ultrastructures. CCM processing provides such an opportunity; we were able to obtain a 3D reconstruction of a

genetically labeled *Drosophila* ORN at nanoscale resolution with quality morphological preservation (Figure 4D). In addition, by combining CCM with Flash-and-Freeze EM (Watanabe et al., 2014) and electron tomography, it is possible to capture the fast morphological changes of genetically labeled vesicles in 3D during synaptic transmission.

Furthermore, CCM is applicable to addressing questions in diverse tissue types, as demonstrated here with cultured mammalian cells or tissues of *Drosophila* antennae and mouse brains. Notably, identical solutions and experimental conditions were used for these different tissues in all core steps (Figure 2). Thus, the protocol described here can likely be readily adapted to cells and tissues of other biological systems. In addition, we demonstrated that CCM can further improve the ultrastructure of an aldehyde-perfused brain compared to chemically fixed counterparts (Figure 3B). Given that aldehyde perfusion is often required for the dissection of deeply embedded or fragile tissues, the compatibility of CCM with aldehyde fixation further broadens the applicability of the method.

MATERIALS AND METHODS

Cultured cells preparation

HEK 293T cells were grown on 1.2 mm diameter punches of Aclar (2 mil thick; Electron Microscopy Sciences, Hatfield, PA) for 48 hours, in a humidified cell culture incubator with 5% CO_2 at 37 °C. The culture medium used was DMEM (Mediatech Inc., Manassas, VA) supplemented with 10% fetal bovine serum (Gemini Bio-Products, West Sacramento, CA). The cells were transfected with Lipofectamine 2000 (Invitrogen, Carlsbad, CA) with a plasmid carrying APEX2 targeted to mitochondria (pcDNA3-Mito-V5-APEX2, Addgene #72480) (Lam et al., 2015). At 24 hours after transfection, the cells were used for CCM processing.

DNA constructs and *Drosophil*a transgenesis

Orco cDNA was a gift from Dr. Aidan Kiely, and APEX2 cDNA was acquired from Addgene (APEX2-NES, #49386). Membrane targeting of APEX2 was achieved by fusing the marker protein to the C-terminus of mCD8GFP or to the N-terminus of Orco. Briefly, gel-purified PCR fragments of mCD8GFP, APEX2, and/or Orco were pieced together with Gibson Assembly following manufacturer's instructions (New England Biolabs, Ipswich, MA). A linker (SGGGG) was added between APEX2 and its respective fusion partner. In the APEX2-Orco construct, a myc tag was included in the primer and added to the N-terminus of APEX2 to enable the detection of the fusion protein by immunostaining. To facilitate Gateway Cloning (ThermoFisher Scientific, Waltham, MA), the attB1 and attB2 sites were included in the primers and added to the ends of the Gibson assembly product by PCR amplification. The PCR products were then purified and cloned into pDONR221 vectors via BP Clonase II (Life Technologies, Carlsbad,

CA). The entry clones were recombined into the pBID-UASC-G destination vector (Wang, Beck and McCabe, PloS ONE, 2012) using LR Clonases II (Life Technologies, Carlsbad, CA).

Drosophila transgenic lines were derived from germline transformations using the ΦC31 integration systems (Groth, Fish, Nusse, & Calos, 2004; Markstein, Pitsouli, Villalta, Celniker, & Perrimon, 2008). All transgenes described in this study were inserted into the attP40 landing site on the second chromosome (BestGene Inc., Chino Hills, CA). Target expression of APEX2 in the ORNs was driven by the Or47b-GAL4 driver (#9984, Bloomington Drosophila Stock Center, Figures 3-5) or the Or22a-GAL4 driver (Dobritsa et al. 2003, Figure 4—video supplement 1). Flies were raised on standard cornmeal food at 25 °C in a 12:12 light-dark cycle.

Drosophila antennae preparation

Six to eight days old flies were cold anesthetized and then pinned to a Sylgard dish. The third segments of the antennae were removed from the head of the fly with a pair of fine forceps and then immediately transferred to a drop of 1X PBS on the dish. With a sharp glass microelectrode, a hole was poked in the antenna to facilitate solution exchange. It is critical that the tissue remained in PBS at all times to prevent deflation. The antenna should remain plump and maintain its shape prior to cryofixation.

Chemical fixation of _Drosophila_ antenna

Antennae were dissected as described above, and then incubated in Karnovsky fixatives (2% paraformaldehyde/2.5% glutaraldehyde/2 mM $CaCl_2$ in 0.1 M sodium cacodylate) at 4°C for 18 hours. Next, samples were washed in 0.1 M sodium cacodylate for 10 minutes and in a

330 solution of 100 mM glycine (Bio-Rad Laboratories, Hercules, CA) in 0.1 M sodium cacodylate for
331 another 10 minutes, and twice more in 0.1 M sodium cacodylate. All washing steps were
332 performed on ice. The following *en bloc* heavy metal staining, dehydration and resin embedding
333 steps were carried out as described in the CryoChem Method section below.

334

335 **Transgenic mice and virus-mediated gene transfer**

336 Animals were handled in accordance with the guidelines established by the *Guide for*
337 *Care and Use of Laboratory Animals* of the National Institutes of Health and approved by the
338 Animal Care and Use Committee of University of California, San Diego. To introduce GFP and
339 tdTomato fluorescent markers in a mouse brain (Figure 5—figure supplement 1), GFP was
340 expressed in the tyrosine hydroxylase (TH)-expressing neurons and tdTomato in the
341 corticotropin releasing factor (CRF)-expressing neurons. A CRF driver mouse line (B6.Cg-
342 $Crh^{tm1(cre)Zjh}$/J, Jackson laboratory) expressing CRE recombinase under the control of the Crh
343 promoter/enhancer elements was first crossed to a tdTomato reporter line (B6.Cg-
344 $Gt.ROSA.26Sor^{tm14(CAG-tdTomato)Hze}$/J, Jackson Laboratory). The progeny was then crossed to a
345 TH-GFP mouse line (Kessler, Yang, Gollomp, Jin, & Iacovitti, 2003), obtaining a transgenic
346 model stably expressing GFP in dopaminergic (TH^+) neurons and CRE/tdTomato in CRF-
347 releasing neurons. To test the 3D CLEM protocol and the morphological preservation offered by
348 CCM (Figure 3B, Figure 6 and Figure 6—video supplement 1), a mouse brain from a tdTomato
349 reporter line (B6.Cg-$Gt.ROSA.26Sor^{tm14(CAG-tdTomato)Hze}$/J, Jackson Laboratory) was used.

350

351

352 **Mouse brain preparation**

353 Mice were anesthetized with ketamine/xylazine and then transcardially perfused with
354 Ringer's solution followed by 0.15 M sodium cacodylate containing 4% paraformaldehyde/0.2%
355 (Figure 5—figure supplement 1) or 0.5% (Figure 3B, Figure 6 and Figure 6—video supplement
356 1) glutaraldehyde/2 mM $CaCl_2$. The animal was perfused for 10 minutes with the fixatives and
357 then the brain was removed and placed in ice-cold fixative for 1 hour. The brain was then cut
358 into 100-µm thick slices using a vibrating microtome. Slices were either processed for chemical
359 fixation (Figure 3B) or stored in ice-cold 0.15 M sodium cacodylate for around 4 hours until used
360 for high-pressure freezing (Figure 3B, Figure 5—figure supplement 1, Figure 6 and Figure 6—
361 video supplement 1).

362

363 **Chemical fixation of mouse brain**

364 The aldehyde-perfused mouse brain slices were post-fixed in 2.5% glutaraldehyde for 20
365 minutes, then washed with 0.15 M sodium cacodylate five times for 5 minutes on ice. Next, the
366 samples were incubated in 0.15 M sodium cacodylate with 100 mM glycine for 5 minutes on ice,
367 then washed in 0.15 M sodium cacodylate similarly. The following *en bloc* heavy metal staining,
368 dehydration and resin embedding steps were carried out as described in the CryoChem Method
369 section below.

370

371

372 **CryoChem Method:**

373 **(I) Cryofixation by high-pressure freezing**

374 *Cultured cells:* Aclar disks were placed within the well of a 100 μm-deep membrane
375 carrier. The cells were covered with the culture medium and then high pressure frozen with a
376 Leica EM Pact 2 unit.

377 *Drosophila antennae*: The third antennal segment was dissected as described above.
378 Antennae from the same fly were transferred into the 100 μm-deep well of a type A planchette
379 filled with 20% BSA (Sigma-Aldrich, St. Louis, MO) in 0.15 M sodium cacodylate. The well of the
380 type A planchette was then covered with the flat side of a type B planchette to secure the
381 sample. The samples were immediately loaded into a freezing holder and frozen with a high-
382 pressure freezing machine (Bal-Tec HPM 010). Planchettes used for cryofixation were pre-
383 coated with 1-hexadecene (Sigma-Aldrich, St. Louis, MO) to prevent planchettes A and B from
384 adhering to each other so as to allow solution to reach the samples during freeze-substitution.

385 *Mouse brain slices*: A 1.2 mm tissue puncher was used to cut a portion of hypothalamus
386 expressing tdTomato (Figure 3B, Figure 5—figure supplement, Figure 6 and Figure 6—video
387 supplement 1) and GFP (Figure 5—figure supplement) from a tissue slice. The tissue punch
388 was placed into a 100 μm-deep membrane carrier and surrounded with 20% BSA in 0.15 M
389 sodium cacodylate. The specimen was high-pressure frozen as described for the *Drosophila*
390 antennae.

391 All frozen samples were stored in liquid nitrogen until further processing.

392

(II) Freeze-substitution

Frozen samples in a planchette were transferred to cryo-vials containing the following freeze-substitution solution: 0.2% glutaraldehyde (#18426, Ted Pella, Redding, CA), 0.1% uranyl acetate (Electron Microscopy Sciences, Hatfield, PA), and 1% water in acetone (#AC326800010, ACROS Organics, USA) in a liquid nitrogen bath. The sample vials were then transferred to a freeze-substitution device (Leica EM AFS2) at -90 °C for 58 hours, from -90 °C to -60 °C for 15 hours (with the temperature raised at 2 °C/hr), at -60 °C for 15 hours, from -60 °C to -30 °C for 15 hours (at +2 °C/hr), and then at -30 °C for 15 hours. In the last hour at -30°C, samples were washed three times in an acetone solution with 0.2% glutaraldehyde and 1% water for 20 minutes. The cryo-tubes containing the last wash were then transferred on ice for an hour.

(III) Rehydration

The freeze-substituted samples were then rehydrated gradually in a series of nine rehydration solutions (see below). The samples were transferred from the freeze-substitution solution to the first rehydration solution (5% water, 0.2% glutaraldehyde in acetone) on ice for 10 minutes. The rehydration step was repeated in a stepwise manner until the samples were fully rehydrated in the final rehydration solution (0.1 M and 0.15 M sodium cacodylate for cells and antennae or mouse brain slices, respectively) (van Donselaar et al., 2007):

1) 5% water, 0.2% glutaraldehyde in acetone
2) 10% water, 0.2% glutaraldehyde in acetone
3) 20% water, 0.2% glutaraldehyde in acetone
4) 30% water, 0.2% glutaraldehyde in acetone
5) 50% 0.1M HEPES (Gibco, Taiwan), 0.2% glutaraldehyde in acetone

6) 70%, 0.1M HEPES, 0.2% glutaraldehyde in acetone

7) 0.1 M HEPES

8) 0.1 M / 0.15 M sodium cacodylate with 100 mM glycine

9) 0.1 M / 0.15 M sodium cacodylate

After rehydration, samples were removed from the planchettes using a pair of forceps under a stereo microscope to a 0.1 M / 0.15 M sodium cacodylate solution in a scintillation vial on ice. It is important that subsequent DAB labeling and *en bloc* heavy metal staining are carried out in scintillation vials instead of the planchettes because metal planchettes may react with the labeling or staining reagents.

(IV) DRAQ5 staining

Mouse brain slices were incubated in DRAQ5 (1:1000 in 0.15 M sodium cacodylate buffer; ThermoFisher Scientific, Waltham, MA) on ice for 60 minutes. Then the samples were washed in 0.15 M sodium cacodylate three times for 10 minutes on ice before fluorescence imaging.

(V) Fluorescence imaging

Drosophila antenna: Freshly dissected or cryofixed-rehydrated antennae (*10x UAS-APEX2-mCD8GFP; Or47b-GAL4*) were mounted in FocusClear (elExplorer, Taiwan) between two cover glasses (#1.5 thickness, 22 mm x 22 mm, Fisher Scientific, Hampton, NH) separated by two layers of spacer rings. Confocal images were collected on an Olympus FluoView 1000 confocal microscope with a 60X water-immersion objective lens. The 488 nm laser was used to excite GFP and all images were acquired at the same laser power and gain to enable comparison between the fresh vs cryofixed-rehydrated samples.

Mouse brain slices: Confocal images of mouse brain slices were collected on a Leica SPE II confocal microscope with a 20X water-immersion objective lens using 488 nm and 561 nm excitation. After freeze-substitution and rehydration, the specimens were placed in ice-cold 0.15 M sodium cacodylate for imaging. Confocal volumes of DRAQ5 and tdTomato signals were collected on an Olympus FluoView 1000 confocal microscope with 20X air and 60X water objectives.

(VI) DAB labeling of target structures by APEX2

Cultured cells: Samples were transferred to a 0.05% DAB (#D5637, Sigma-Aldrich, St. Louis, MO) solution in 0.1 M sodium cacodylate for 5 minutes on ice to allow DAB to diffuse into the tissue. To label the mitochondria in the APEX2-expressing cells, samples were then transferred to a 0.05% DAB solution with 0.015% H_2O_2 (Fisher Scientific, Hampton, NH) in 0.1 M sodium cacodylate until DAB labeling was visible under a microscope (~5 minutes on ice). After the reaction, samples were washed three times with 0.1 M sodium cacodylate on ice for 10 minutes.

Drosophila antennae: Samples were first placed into a 0.05% DAB solution in 0.1 M sodium cacodylate for an hour on ice to allow DAB to access target neurons underneath the cuticle in the antenna. To label APEX2-expressing ORNs, antennae were then transferred into a 0.05% DAB solution with 0.015% H_2O_2 in 0.1 M sodium cacodylate for an hour on ice. After the reaction, samples were washed three times with 0.1 M sodium cacodylate on ice for 10 minutes.

(VII) *En bloc* heavy metal staining for TEM and SBEM

For TEM: Cultured cells and mouse brain slices were incubated in 2% OsO_4 (Electron Microscopy Sciences, Hatfield, PA) /1.5% potassium ferrocyanide (Mallinckrodt, Staines-Upon-Thames, UK) /2 mM $CaCl_2$ in 0.1 M (cells) or 0.15 M (brain) sodium cacodylate for an hour on

ice. Then samples were washed in water five times for 5 minutes on ice prior to the dehydration step detailed below.

For SBEM: *Drosophila* antennae and mouse brain slices were incubated in 2% OsO_4/1.5% potassium ferrocyanide/2 mM $CaCl_2$ in 0.1 M (antennae) or 0.15 M (brain) sodium cacodylate for an hour at room temperature. Then samples were washed in water five times for 5 minutes and transferred to 0.5% thiocarbohydrazide (filtered with 0.22 µm filter before use; Electron Microscopy Sciences, Hatfield, PA) for 30 minutes at room temperature. Samples were washed in water similarly and incubated in 2% OsO_4 for 30 minutes at room temperature. Afterwards, samples were rinsed with water, then transferred to 2% aqueous uranyl acetate (filtered with 0.22 µm filter) at 4 °C overnight. In the next morning, samples were first washed in water five times for 5 minutes and then subjected to the dehydration steps detailed below.

(VIII) Dehydration

Samples were dehydrated with a series of ethanol solutions and acetone in six steps of 10 minutes each: 70% ethanol, 90% ethanol, 100% ethanol, 100% ethanol, 100% acetone, 100% acetone. All ethanol dehydration steps were carried out on ice, and the acetone steps at room temperature. The first acetone dehydration step was carried out with ice-cold acetone, and the second one was with acetone kept at room temperature.

(IX) Resin infiltration

Cultured cells: Samples were transferred to a Durcupan ACM resin/acetone (1:1) solution for an hour on a shaker at room temperature. The samples were then transferred to fresh 100% Durcupan ACM resin overnight and subsequently placed in fresh resin for four hours. While in 100% resin, samples were placed in a vacuum chamber on a rocker to facilitate

the removal of residual acetone. Finally, the samples were embedded in fresh resin at 60 °C for two days.

Drosophila antennae and mouse brain slices: Samples were transferred to a Durcupan ACM resin/acetone (1:1) solution overnight on a shaker. The next day, samples were transferred into fresh 100% Durcupan ACM resin twice, with six to seven hours apart. While in 100% resin, samples were placed in a vacuum chamber on a rocker to facilitate the removal of residual acetone. After the overnight incubation in 100% resin, samples were embedded in fresh resin at 60 °C for at least two days.

Durcupan ACM resin (Sigma Aldrich, St. Louis, MO) composition was 11.4 g component A, 10 g component B, 0.3 g component C, and 0.1 g component D.

X-ray Microscopy (microcomputed tomography)

Drosophila antenna: Microcomputed tomography (microCT) was performed on resin-embedded specimens using a Versa 510 X-ray microscope (Zeiss). Flat-embedded specimens were glued to the end of an aluminum rod using cyanoacrylic glue. Imaging was performed with a 40X objective using a tube current of 40 kV and no source filter. Raw data consisted of 1601 projection images collected as the specimen was rotated 360 degrees. The voxel dimension of the final tomographic reconstruction was 0.4123 µm.

Mouse brain slices: X-ray microscopy scan was collected of a resin-embedded sample at 80 kVp with a voxel size of 0.664 µm prior to mounting for SBEM imaging. A second scan was collected of the mounted specimen at 80 kVp with 0.7894 µm voxels.

505 **Transmission Electron Microscopy**

506 Ultrathin sections (70 nm) were collected on 300 mesh copper grids. Samples were
507 post-stained with either Sato's lead solution only (cultured cells) or with 2% uranyl acetate and
508 Sato's lead solution (mouse brain slices). Sections were imaged on an FEI Spirit TEM at 80 kV
509 equipped with a 2k x 2k Tietz CCD camera.

510

511 **Serial Block-face Scanning Electron Microscopy**

512 *Drosophila antenna*: Following microcomputed tomography to confirm proper orientation
513 of region of interest, specimens were mounted on aluminum pins with conductive silver epoxy
514 (Ted Pella, Redding, CA). The specimens were trimmed to remove excess resin above ROI and
515 to remove silver epoxy from sides of specimen. The specimens were sputter coated with gold-
516 palladium and then imaged using a Gemini scanning electron microscope (Zeiss) equipped with
517 a 3View2XP and OnPoint backscatter detector (Gatan). Images were acquired at 2.5 kV
518 accelerating voltage with a 30 µm condenser aperture and 1 µsec dwell time; Z step size was
519 50 nm. Volumes were either collected in variable pressure mode with a chamber pressure of 30
520 Pa and a pixel size of 3.8 nm (Figure 3—video supplement 1 and Figure 4D) or using local gas
521 injection (Deerinck et al., 2017) set to 85% and a pixel size of 6.5 nm (Figures 3A and 4C).
522 Volumes were aligned using cross correlation, segmented, and visualized using IMOD.

523 *Mouse brain slices:* SBEM was performed on a Merlin scanning electron microscope
524 (Zeiss) equipped with a 3View2XP and OnPoint backscatter detector (Gatan). The volume was
525 collected at 2 kV, with 6.8 nm pixels and 70 nm Z steps. Local gas injection (Deerinck et al.,
526 2017) was set to 15% during imaging. The raster size was 10k x 15k and the Z dimension was
527 659 sections.

528

529 **Semi-automated segmentation of DAB-labeled *Drosophila* olfactory receptor neuron**

530 The DAB-labeled *Drosophila* ORN was segmented in a semi-automated fashion using
531 the IMOD software (Kremer, Mastronarde, & McIntosh, 1996) to generate the 3D model. The
532 IMOD command line 'imodauto' was used for the auto-segmentation by setting thresholds to
533 isolate the labeled cellular structures of interest. Further information about the utilities of
534 'imodauto' can be found in the IMOD manual
535 (http://bio3d.colorado.edu/imod/doc/man/imodauto.html). Auto-segmentation was followed by
536 manual proofreading and reconstruction by two independent proofreaders. The proofreaders
537 used elementary operations in IMOD, most commonly the 'drawing tools' to correct the contours
538 generated by 'imodauto'. Where 'imodauto' failed to be applied successfully, the proofreaders
539 also used the 'drawing tools' to directly trace the outline of the labeled structure. The contours of
540 ORNs generally do not vary markedly between adjacent sections. Therefore, alternate sections
541 were traced for the reconstruction of some parts of the ORN dendrite.

542

543 **Quantification of fluorescence intensity**

544 To quantify GFP fluorescence intensity shown in Figure 5, maximum intensity Z-
545 projections were generated using ImageJ (NIH). Average fluorescence intensity in the
546 background was subtracted from the fluorescence intensity of each cell body measured. Only
547 non-overlapping cell bodies were quantified. Kolmogorov-Smirnov Test was performed on
548 http://www.physics.csbsju.edu/stats/KS-test.html and Mann-Whitney *U* Test was performed
549 using SigmaPlot 13.0 (Systat Software, San Jose, CA).

550

551 **Light and electron microscope volume registration**

552 To target tdTomato-expressing cells in the mouse brain for SBEM imaging, the confocal
553 volumes collected in the frozen-rehydrated specimen was registered with the microCT volume
554 of the resin-embedded sample, using a software tool developed in our lab. The resin-embedded
555 specimen was then mounted and trimmed for SBEM based on the microCT volume. A second
556 microCT scan of the mounted specimen allowed for precise targeting of the cells of interest with
557 the Gatan stage for SBEM. After the SBEM volume was collected, the confocal and SBEM
558 volumes were registered using the landmark tool of Amira 6.3 (ThermoFisher, Waltham, MA).
559 Heterochromatin structures revealed by DRAQ5 labeling and visible in the SBEM volume were
560 used as landmark points for the registration.

REFERENCES

Briggman, K. L., & Bock, D. D. (2012). Volume electron microscopy for neuronal circuit reconstruction. *Current Opinion in Neurobiology*, *22*(1), 154–161. http://doi.org/10.1016/j.conb.2011.10.022

Brown, E., Mantell, J., Carter, D., Tilly, G., & Verkade, P. (2009). Studying intracellular transport using high-pressure freezing and Correlative Light Electron Microscopy. *Seminars in Cell and Developmental Biology*, *20*(8), 910–919. http://doi.org/10.1016/j.semcdb.2009.07.006

Bushong, E. A., Johnson, D. D., Kim, K.-Y., Terada, M., Hatori, M., Peltier, S. T., Panda, S., Merkle, A., Ellisman, M. H. (2015). X-Ray Microscopy as an Approach to Increasing Accuracy and Efficiency of Serial Block-Face Imaging for Correlated Light and Electron Microscopy of Biological Specimens. *Microscopy and Microanalysis*, *21*(1), 231–238. http://doi.org/10.1017/S1431927614013579

Dahl, R., & Staehelin, L. A. (1989). High-pressure freezing for the preservation of biological structure: Theory and practice. *Journal of Electron Microscopy Technique*, *13*(3), 165–174. http://doi.org/10.1002/jemt.1060130305

de Boer, P., Hoogenboom, J. P., & Giepmans, B. N. G. (2015). Correlated light and electron microscopy: Ultrastructure lights up! *Nature Methods*, *12*(6), 503–513. http://doi.org/10.1038/nmeth.3400

Deerinck, T., Bushong, E., Lev-Ram, V., Shu, X., Tsien, R., & Ellisman, M. (2010). Enhancing Serial Block-Face Scanning Electron Microscopy to Enable High Resolution 3-D Nanohistology of Cells and Tissues. *Microscopy and Microanalysis*, *16*(S2), 1138–1139. http://doi.org/10.1017/S1431927610055170

Deerinck, T. J., Shone, T. M., Bushong, E. A., Ramachandra, R., Peltier, S. T., & Ellisman, M. H. (2017). High-performance serial block-face SEM of nonconductive biological samples

585 enabled by focal gas injection-based charge compensation. *Journal of Microscopy*, *0*(0), 1–
586 8. http://doi.org/10.1111/jmi.12667

587 Denk, W., & Horstmann, H. (2004). Serial block-face scanning electron microscopy to
588 reconstruct three-dimensional tissue nanostructure. *PLoS Biology*, *2*(11), e329.
589 http://doi.org/10.1371/journal.pbio.0020329

590 Ding, R. (1993). Three-dimensional reconstruction and analysis of mitotic spindles from the
591 yeast, Schizosaccharomyces pombe. *The Journal of Cell Biology*, *120*(1), 141–151.
592 http://doi.org/10.1083/jcb.120.1.141

593 Dobritsa, A. A, van der Goes van Naters, W., Warr, C. G., Steinbrecht, R. A., & Carlson, J. R.
594 (2003). Integrating the molecular and cellular basis of odor coding in the Drosophila
595 antenna. *Neuron*, *37*(5), 827–41. http://www.ncbi.nlm.nih.gov/pubmed/12628173

596 Doroquez, D. B., Berciu, C., Anderson, J. R., Sengupta, P., & Nicastro, D. (2014). A high-
597 resolution morphological and ultrastructural map of anterior sensory cilia and glia in
598 Caenorhabditis elegans. *eLife*, *2014*(3), 1–35. http://doi.org/10.7554/eLife.01948

599 Ellisman, M. H., Deerinck, T. J., Kim, K. Y., Bushong, E. A., Phan, S., Ting, A. Y., & Boassa, D.
600 (2015). Advances in molecular probe-based labeling tools and their application to
601 multiscale multimodal correlated microscopies. *Journal of Chemical Biology*.
602 http://doi.org/10.1007/s12154-015-0132-6

603 Gaietta, G., Deerinck, T. J., Adams, S. R., Bouwer, J., Tour, O., Laird, D. W., Sosinsky, G. E.,
604 Tsien, R. Y., Ellisman, M. H. (2002). Multicolor and electron microscopic imaging of
605 connexin trafficking. *Science*, *296*(5567), 503–507. http://doi.org/10.1126/science.1068793

606 Groth, A. C., Fish, M., Nusse, R., & Calos, M. P. (2004). Construction of Transgenic Drosophila
607 by Using the Site-Specific Integrase from Phage ΦC31. *Genetics*, *166*(4), 1775–1782.
608 http://doi.org/10.1534/genetics.166.4.1775

609 Hess, M. W., Müller, M., Debbage, P. L., Vetterlein, M., & Pavelka, M. (2000). Cryopreparation
610 provides new insight into the effects of brefeldin A on the structure of the HepG2 Golgi
611 apparatus. *Journal of Structural Biology*, *130*(1), 63–72.
612 http://doi.org/10.1006/jsbi.2000.4230

613 Joesch, M., Mankus, D., Yamagata, M., Shahbazi, A., Schalek, R., Suissa-Peleg, A., Meister,
614 M., Lichtman, J. W., Scheirer, W. J., Sanes, J. R. (2016). Reconstruction of genetically
615 identified neurons imaged by serial-section electron microscopy. *eLife*, *5*(e15015), 1-13.
616 http://doi.org/10.7554/eLife.15015

617 Kaeser, W., Koyro, H. -W, & Moor, H. (1989). Cryofixation of plant tissues without pretreatment.
618 *Journal of Microscopy*, *154*(3), 279–288. http://doi.org/10.1111/j.1365-2818.1989.tb00591.x

619 Kellenberger, E., Johansen, R., Maeder, M., Bohrmann, B., Stauffer, E., & Villiger, W. (1992).
620 Artefacts and morphological changes during chemical fixation. *Journal of Microscopy*,
621 *168*(2), 181–201. http://doi.org/10.1111/j.1365-2818.1992.tb03260.x

622 Kelley, R. O., Dekker, R. A. F., & Bluemink, J. G. (1973). Ligand-mediated osmium binding: Its
623 application in coating biological specimens for scanning electron microscopy. *Journal of*
624 *Ultrasructure Research*, *45*(3–4), 254–258. http://doi.org/10.1016/S0022-5320(73)80051-6

625 Kessler, M. A, Yang, M., Gollomp, K. L., Jin, H., & Iacovitti, L. (2003). The human tyrosine
626 hydroxylase gene promoter. *Molecular Brain Research*, *112*(1–2), 8–23.
627 http://doi.org/10.1016/S0169-328X(02)00694-0

628 Kiss, J. Z., Giddings, T. H., Staehelin, L. A., & Sack, F. D. (1990). Comparison of the
629 ultrastructure of conventionally fixed and high pressure frozen/freeze substituted root tips
630 of Nicotiana and Arabidopsis. *Protoplasma*, *157*(1–3), 64–74.
631 http://doi.org/10.1007/BF01322639

632 Kolotuev, I., Schwab, Y., & Labouesse, M. (2010). A precise and rapid mapping protocol for

correlative light and electron microscopy of small invertebrate organisms. *Biology of the Cell*, *102*(2), 121–132. http://doi.org/10.1042/BC20090096

Korogod, N., Petersen, C. C. H., & Knott, G. W. (2015). Ultrastructural analysis of adult mouse neocortex comparing aldehyde perfusion with cryo fixation. *eLife*, *4*(e05793), 1–17. http://doi.org/10.7554/eLife.05793

Kremer, J. R., Mastronarde, D. N., & McIntosh, J. R. (1996). Computer Visualization of Three-Dimensional Image Data Using IMOD. *Journal of Structural Biology*, *116*(1), 71–76. http://doi.org/10.1006/jsbi.1996.0013

Kukulski, W., Schorb, M., Welsch, S., Picco, A., Kaksonen, M., & Briggs, J. A. G. (2011). Correlated fluorescence and 3D electron microscopy with high sensitivity and spatial precision. *Journal of Cell Biology*, *192*(1), 111–119. http://doi.org/10.1083/jcb.201009037

Lam, S. S., Martell, J. D., Kamer, K. J., Deerinck, T. J., Ellisman, M. H., Mootha, V. K., & Ting, A. Y. (2015). Directed evolution of APEX2 for electron microscopy and proximity labeling. *Nature Methods*, *12*(1), 51–54. http://doi.org/10.1038/nmeth.3179

Leapman, R. D. (2004). Novel techniques in electron microscopy. *Current Opinion in Neurobiology*, *14*(5), 591–598. http://doi.org/10.1016/j.conb.2004.08.004

Markstein, M., Pitsouli, C., Villalta, C., Celniker, S. E., & Perrimon, N. (2008). Exploiting position effects and the gypsy retrovirus insulator to engineer precisely expressed transgenes. *Nature Genetics*, *40*(4), 476–483. http://doi.org/10.1038/ng.101

Martell, J. D., Deerinck, T. J., Sancak, Y., Poulos, T. L., Mootha, V. K., Sosinsky, G. E., … Ting, A. Y. (2012). Engineered ascorbate peroxidase as a genetically encoded reporter for electron microscopy. *Nature Biotechnology*, *30*(11), 1143–8. http://doi.org/10.1038/nbt.2375

McDonald, K. (1999). High-Pressure Freezing for Preservation of High Resolution Fine

Structure and Antigenicity for Immunolabeling. In *Electron Microscopy Methods and Protocols* (Vol. 117, pp. 77–98). New Jersey: Humana Press. http://doi.org/10.1385/1-59259-201-5:77

McDonald, K. (2007). Cryopreparation Methods for Electron Microscopy of Selected Model Systems. *Methods in Cell Biology*. http://doi.org/10.1016/S0091-679X(06)79002-1

McDonald, K. (2009). A review of high-pressure freezing preparation techniques for correlative light and electron microscopy of the same cells and tissues. *Journal of Microscopy*, *235*(3), 273–281. http://doi.org/10.1111/j.1365-2818.2009.03218.x

Moor, H. (1987). Theory and Practice of High Pressure Freezing. In R. A. Steinbrecht & K. Zierold (Eds.), *Cryotechniques in Biological Electron Microscopy* (pp. 175–191). Berlin, Heidelberg: Springer Berlin Heidelberg. http://doi.org/10.1007/978-3-642-72815-0_8

Müller-Reichert, T., Hohenberg, H., O'Toole, E. T., & Mcdonald, K. (2003). Cryoimmobilization and three-dimensional visualization of C. elegans ultrastructure. *Journal of Microscopy*, *212*(1), 71–80. http://doi.org/10.1046/j.1365-2818.2003.01250.x

Ng, J., Browning, A., Lechner, L., Terada, M., Howard, G., Jefferis, G. S. X. E. (2016). Genetically targeted 3D visualisation of Drosophila neurons under Electron Microscopy and X-Ray Microscopy using miniSOG. *Scientific Reports*, *6*(1), 38863. http://doi.org/10.1038/srep38863

Ngo, J. T., Adams, S. R., Deerinck, T. J., Boassa, D., Rodriguez-Rivera, F., Palida, S. F., Carolyn, R. B., Ellisman, M. H., Tsien, R. Y. (2016). Click-EM for imaging metabolically tagged nonprotein biomolecules. *Nature Chemical Biology*, *12*(6), 459–465. http://doi.org/10.1038/nchembio.2076

Nixon, S. J., Webb, R. I., Floetenmeyer, M., Schieber, N., Lo, H. P., Parton, R. G. (2009). A single method for cryofixation and correlative light, electron microscopy and tomography of

zebrafish embryos. *Traffic*, *10*(2), 131–136. http://doi.org/10.1111/j.1600-0854.2008.00859.x

Ou, H. D., Phan, S., Deerinck, T. J., Thor, A., Ellisman, M. H., O'Shea, C. C. (2017). ChromEMT: Visualizing 3D chromatin structure and compaction in interphase and mitotic cells. *Science*, *357*(6349), eaag0025. http://doi.org/10.1126/science.aag0025

Ryan, K., Lu, Z., Meinertzhagen, I. A. (2016). The CNS connectome of a tadpole larva of Ciona intestinalis (L.) highlights sidedness in the brain of a chordate sibling. *eLife*, *5*(e16962), 1–34. http://doi.org/10.7554/eLife.16962

Sabatini, D. D. (1963). CYTOCHEMISTRY AND ELECTRON MICROSCOPY: The Preservation of Cellular Ultrastructure and Enzymatic Activity by Aldehyde Fixation. *The Journal of Cell Biology*, *17*(1), 19–58. http://doi.org/10.1083/jcb.17.1.19

Schwarz, H., Humbel, B. (2009). Correlative light and electron microscopy. In A. Cavalier, D. Spehner, B. Humbel (Eds.), *Handbook of cryo-preparation methods for electron microscopy.* (pp. 537–565). CRC Press.

Shanbhag, S. R., Müller, B., Steinbrecht, R. A. (1999). Atlas of olfactory organs of Drosophila melanogaster 1. Types, external organization, innervation and distribution of olfactory sensilla. *International Journal of Insect Morphology and Embryology*, *28*(4), 377–397. http://doi.org/10.1016/S0020-7322(99)00039-2

Shanbhag, S. R., Müller, B., Steinbrecht, R. A. (2000). Atlas of olfactory organs of Drosophila melanogaster 2. Internal organization and cellular architecture of olfactory sensilla. *Arthropod Structure & Development*, *29*(3), 211–229. http://doi.org/10.1016/S1467-8039(00)00028-1

Shaner, N. C., Campbell, R. E., Steinbach, P. A., Giepmans, B. N. G., Palmer, A. E., Tsien, R. Y. (2004). Improved monomeric red, orange and yellow fluorescent proteins derived from

Discosoma sp. red fluorescent protein. *Nature Biotechnology*, *22*(12), 1567–1572. http://doi.org/10.1038/nbt1037

Shimoni, E., Müller, M., Mueller, M. (1998). On optimizing high-pressure freezing: from heat transfer theory to a new mircrobiopsy device. *Journal of Microscopy*, *192*(Pt 3), 236–247. Retrieved from http://www.ncbi.nlm.nih.gov/pubmed/9923416

Shu, X., Lev-Ram, V., Deerinck, T. J., Qi, Y., Ramko, E. B., Davidson, M. W., Jin, Y., Ellisman, M. H., Tsien, R. Y. (2011). A genetically encoded tag for correlated light and electron microscopy of intact cells, tissues, and organisms. *PLoS Biology*, *9*(4), e1001041. http://doi.org/10.1371/journal.pbio.1001041

Sosinsky, G. E., Crum, J., Jones, Y. Z., Lanman, J., Smarr, B., Terada, M., Martone, M. E., Deerinck, T. J., Johnson, J. E., Ellisman, M. H. (2008). The combination of chemical fixation procedures with high pressure freezing and freeze substitution preserves highly labile tissue ultrastructure for electron tomography applications. *Journal of Structural Biology*, *161*(3), 359–371. http://doi.org/10.1016/j.jsb.2007.09.002

Steinbrecht, R. A. (1980). Cryofixation without cryoprotectants. Freeze substitution and freeze etching of an insect olfactory receptor. *Tissue and Cell*, *12*(1), 73–100. http://doi.org/10.1016/0040-8166(80)90053-1

Steinbrecht, R. A., Müller, M. (1987). Freeze-Substitution and Freeze-Drying. In R. A. Steinbrecht & K. Zierold (Eds.), *Cryotechniques in Biological Electron Microscopy* (pp. 149–172). Berlin, Heidelberg: Springer Berlin Heidelberg. http://doi.org/10.1007/978-3-642-72815-0_7

Szczesny, P. J., Walther, P., Müller, M. (1996). Light damage in rod outer segments: The effects of fixation on ultrastructural alterations. *Current Eye Research*, *15*(8), 807–814. http://doi.org/10.3109/02713689609017621

729 Takemura, S., Bharioke, A., Lu, Z., Nern, A., Vitaladevuni, S., Rivlin, P. K., … Chklovskii, D. B.
730 (2013). A visual motion detection circuit suggested by Drosophila connectomics. *Nature*,
731 *500*(7461), 175–181. http://doi.org/10.1038/nature12450

732 Tapia, J. C., Kasthuri, N., Hayworth, K. J., Schalek, R., Lichtman, J. W., Smith, S. J., Buchanan,
733 J. (2012). High-contrast en bloc staining of neuronal tissue for field emission scanning
734 electron microscopy. *Nature Protocols*, *7*(2), 193–206.
735 http://doi.org/10.1038/nprot.2011.439

736 van Donselaar, E., Posthuma, G., Zeuschner, D., Humbel, B. M., Slot, J. W. (2007).
737 Immunogold labeling of cryosections from high-pressure frozen cells. *Traffic*, *8*(5), 471–
738 485. http://doi.org/10.1111/j.1600-0854.2007.00552.x

739 Watanabe, S., Davis, M. W., & Jorgensen, E. M. (2014). Flash-and-Freeze Electron Microscopy:
740 Coupling Optogenetics with High-Pressure Freezing. In U. V. Nägerl & A. Triller (Eds.),
741 *Nanoscale Imaging of Synapses. Neuromethods* (pp. 43–57). New York, NY: Humana
742 Press. http://doi.org/10.1007/978-1-4614-9179-8_3

743 Watanabe, S., Liu, Q., Davis, M. W., Hollopeter, G., Thomas, N., Jorgensen, N. B., Jorgensen,
744 E. M. (2013). Ultrafast endocytosis at Caenorhabditis elegans neuromuscular junctions.
745 *eLife*, *2013*(2), 1–24. http://doi.org/10.7554/eLife.00723

746 Watanabe, S., Punge, A., Hollopeter, G., Willig, K. I., Hobson, R. J., Davis, M. W., Hell, S. W.,
747 Jorgensen, E. M. (2011). Protein localization in electron micrographs using fluorescence
748 nanoscopy. *Nature Methods*, *8*(1), 80–84. http://doi.org/10.1038/nmeth.1537

749 Watanabe, S., Rost, B. R., Camacho-Pérez, M., Davis, M. W., Söhl-Kielczynski, B.,
750 Rosenmund, C., Jorgensen, E. M. (2013). Ultrafast endocytosis at mouse hippocampal
751 synapses. *Nature*, *504*(7479), 242–247. http://doi.org/10.1038/nature12809

752 Watanabe, S., Trimbuch, T., Camacho-Pérez, M., Rost, B. R., Brokowski, B., Söhl-Kielczynski,

753 B., Felies, A., Davis, M. W., Rosenmund, C., Jorgensen, E. M. (2014). Clathrin regenerates
754 synaptic vesicles from endosomes. *Nature*, *515*(7526), 228–233.
755 http://doi.org/10.1038/nature13846

756 West, J. B., Fu, Z., Deerinck, T. J., Mackey, M. R., Obayashi, J. T., Ellisman, M. H. (2010).
757 Structure-function studies of blood and air capillaries in chicken lung using 3D electron
758 microscopy. *Respiratory Physiology and Neurobiology*, *170*(2), 202–209.
759 http://doi.org/10.1016/j.resp.2009.12.010

760 Williams, M. E., Wilke, S. A., Daggett, A., Davis, E., Otto, S., Ravi, D., Ripley, B., Bushong, E.
761 A., Ellisman, M. H., Klein, G., Ghosh, A. (2011). Cadherin-9 regulates synapse-specific
762 differentiation in the developing hippocampus. *Neuron*, *71*(4), 640–655.
763 http://doi.org/10.1016/j.neuron.2011.06.019

764 Winey, M., Mamay, C. L., O'Toole, E. T., Mastronarde, D. N., Giddings, T. H., McDonald, K. L.,
765 McIntosh, J. R. (1995). Three-dimensional ultrastructural analysis of the Saccharomyces
766 cerevisiae mitotic spindle. *Journal of Cell Biology*, *129*(6), 1601–1615.
767 http://doi.org/10.1083/jcb.129.6.1601

768 Zheng, Z., Lauritzen, J. S., Perlman, E., Robinson, C. G., Nichols, M., Milkie, D., … Bock, D. D.
769 (2017). A Complete Electron Microscopy Volume Of The Brain Of Adult Drosophila
770 melanogaster. *bioRxiv*. http://doi.org/doi.org/10.1101/140905

ACKNOWLEDGEMENTS

We thank Aiden Keily for providing the Orco cDNA construct and R. Alexander Steinbrecht for advice on electron microscopy of *Drosophila* antennae. We also thank Edie Zhang and Martin Orden for assistance in segmentation of *Drosophila* olfactory receptor neuron. We also thank Andrea Thor and Mason Mackey for help with EM sample preparation and imaging. We also thank Steven Wasserman for comments on the manuscript.

FIGURE LEGENDS

Figure 1. Comparison of the advantages and limitations of different sample preparation methods for electron microscopy. The CryoChem Method (CCM) combines the advantages of chemical fixation and cryofixation. With CCM, samples are fixed with high-pressure freezing and freeze-substitution to achieve quality ultrastructural preservation. This approach allows preservation of tissues with cuticle or cell wall and captures biological events with high temporal resolution. A rehydration step is introduced to enable fluorescence imaging, DAB labeling by genetically encoded EM tags and high-contrast *en bloc* heavy metal staining of the cryofixed sample. The high-contrast *en bloc* heavy metal staining permitted by CCM reduces the need for post-staining on sections, and makes CCM compatible with serial block-face scanning electron microscopy (SBEM). Common limitations of chemical fixation and cryofixation are denoted in red.

Figure 2. Flowchart of the CryoChem Method. After cryofixation by high-pressure freezing and freeze-substitution, cryofixed samples are rehydrated gradually. Rehydrated samples can then be imaged for fluorescence, subjected to DAB labeling reaction or *en bloc* stained with a substantial amount of heavy metals. The protocol is modular; the first three processes are the core steps of CCM and the starred steps are optional depending on the experimental design. The samples are then dehydrated for resin infiltration and embedding, followed by imaging with any EM technique of choice. Blue and grey denote hydrated and dehydrated states of the sample, respectively.

Figure 3. CryoChem Method offers high-quality ultrastructural preservation and sufficient *en bloc* staining for SBEM. TEM and SBEM images were acquired to assess the morphology of CCM-processed tissues. (A) The microlamella structures were well-preserved in CCM-

processed *Drosophila* antenna (top right panel), compared to chemically fixed samples (top left panel). In the enlarged views of the boxed regions (bottom panels), the microlamellae in the CCM-processed antenna appeared uniform in size and shape, unlike the chemically fixed ones which were distorted. Scale bars: 1 μm for top panels, 200 nm for bottom panels. (B) CCM enhanced the morphological preservation of aldehyde-perfused mouse brain (top right panel), compared to the chemically fixed control (top left panel). In the enlarged views of the boxed regions (bottom panels), the nuclear membranes (arrows) are smoother in the CCM-processed sample. We note that the chromatin was more heavily stained in the CCM-processed specimen, likely due to the additional exposure to uranyl acetate during freeze substitution. Scale bars: 500 nm for top panels, 100 nm for bottom panels.

Figure supplement 1 for Figure 3. TEM images showed well-preserved ultrastructures in the CCM-processed HEK 293T cells. In the enlarged view of the boxed region (bottom panel), smooth nuclear membranes were observed. Scale bars: 1 μm for the top panel, 500 nm for the bottom panel.

Video supplement 1 for Figure 3. A SBEM volume from a CryoChem-processed *Drosophila* antenna. Scale bar: 500 nm.

Figure 4. CryoChem Method enables DAB labeling by APEX2 in cryofixed tissues. In CCM-processed cultured cells and *Drosophila* antennae, DAB labeling was observed in cells expressing APEX2. (A) Mitochondria expressing APEX2 were labeled with DAB in a transfected HEK 293T cell. (B) An untransfected control cell. Scale bars: 200 nm. (C) An APEX2-expressing olfactory receptor neuron (ORN) was labeled with DAB (arrow) in the *Drosophila* antenna. Asterisks denote ORNs without APEX2 expression. Scale bar: 500 nm. (D) A series of SBEM images showing the same DAB labeled *Drosophila* ORN (arrow) in different planes of section. Asterisks denote ORNs without APEX2 expression. The images were acquired using standard imaging methods without charge compensation by nitrogen gas injection (Deerinck et al., 2017).

These images, together with the rest of the EM volume acquired using SBEM, enabled semi-automatic segmentation and 3D reconstruction of the labeled ORN (right panel). Scale bars: 500 nm for SBEM images, 2 μm for the 3D model of ORN.

Video supplement 1 for Figure 4. An X-ray micro-computed tomography volume from a CCM-processed *Drosophila* antenna showing DAB labeling in subsets of ORNs expressing APEX2. The damaged region on the opposite side of the labeled cells indicates the hole poked in the antenna to facilitate solution exchange. Scale bar: 30 μm.

Figure 5. GFP fluorescence is well-preserved in CryoChem-processed samples. Confocal images were taken to quantify the level of GFP fluorescence in *Drosophila* ORNs. Antennae were collected from transgenic flies expressing GFP in a subset of ORNs. (A) GFP fluorescence intensity distributions of the ORN soma in freshly-dissected, unfixed antennae (left panel) and CCM-processed antennae (right panel) are not significantly different. p=0.810, Kolmogorov-Smirnov test. Insets show representative images, with ORN soma outlined. Scale bar: 2 μm. (B) Comparison of the average fluorescence intensities. GFP intensities are virtually identical between neurons in unfixed antennae and frozen-rehydrated antennae. n=3 antennae for each condition, Error bars denote SEM, p=0.950, Mann-Whitney *U* Test.

Figure supplement 1 for Figure 5. GFP and tdTomato fluorescence in a cryofixed-rehydrated mouse brain. (A) GFP- and (B) tdTomato-positive neurons. (C) Co-expression of GFP and tdTomato fluorescence was detected in the cryofixed-rehydrated mouse brain. Scale bar: 50 μm.

Figure 6. 3D correlated light and electron microscopy (CLEM) in CCM-processed mouse brain. Mouse brain slices with fluorescently labeled neurons were processed with CCM, imaged with confocal microscopy, X-ray microscopy and SBEM for 3D CLEM. (A) Flowchart for performing 3D CLEM with CCM-processed samples. Similar to a typical CCM protocol, the

854 cryofixed sample is first freeze-substituted and rehydrated. The frozen-rehydrated sample is
855 then stained with DRAQ5 to label DNA in the nuclei. Next, the region of interest (ROI) is
856 identified using confocal microscopy based on fluorescent signals, while the DRAQ5 signals are
857 also acquired to serve as fiducial markers. Subsequently, the sample is stained, dehydrated and
858 embedded for X-ray microscopy and SBEM. Using the DRAQ5 signals as fiducial markers, the
859 confocal volumes can be registered to the X-ray volume such that the ROI for SBEM can be
860 identified. Once the SBEM volume is acquired, it can be registered to the confocal volumes
861 based on the positions of the nuclei for 3D CLEM. (B) An example of the DRAQ5 fluorescence
862 signals (left), the corresponding ROI in X-ray volume (middle) and overlay (right). This image
863 registration process facilitates ROI identification in SBEM. Scale bar: 20 μm. (C) DRAQ5
864 fluorescence labeling served as fiducial points for registering the confocal volume to the SBEM
865 volume. Scale bar: 5 μm. (D) The cell body of a tdTomato-expressing neuron (left) was
866 identified in the SBEM volume (middle) through 3D CLEM (right). (E) Neuronal processes
867 expressing tdTomato (left) were also identified in the SBEM volume (middle) through 3D CLEM
868 (right). Scale bars: 2 μm, for both (D) and (E).
869 **Video supplement 1 for Figure 6.** A volume showing 3D CLEM in a CCM-processed mouse
870 brain. tdTomato-expressing neurons were clearly identified in the SBEM volume. Scale bar: 10
871 μm.

SOURCE DATA FILES

Figure 5-Source Data 1 GFP fluorescence intensities in fresh and CCM-processed *Drosophila* antennae.

Figure 1

	Chemical fixation	Cryofixation	CryoChem
Fixation	Aldehyde fixatives (4°C)	1) High pressure freezing (-196°C, ~2100 bar) 2) Freeze-substitution in organic solvents	1) High pressure freezing (-196°C, ~2100 bar) 2) Freeze-substitution in organic solvents
Ultrastructural preservation	Fair	Excellent	Excellent
Tissues with cuticle or cell wall	Incompatible	Compatible	Compatible
Temporal resolution of events captured	Low	High	High
Hydration state of the sample	Hydrated	Dehydrated after freeze substitution	Hydrated after rehydration
Fluorescence imaging after fixation	Compatible	Generally incompatible	Compatible
DAB labeling by genetic EM tags	Compatible	Incompatible due to dehydration	Compatible due to rehydration
High-contrast *en bloc* heavy metal staining	Compatible	Limited	Compatible due to rehydration
Post-staining on sections	Optional	Often required	Optional
SBEM compatibility	Compatible	Incompatible	Compatible

Figure 2

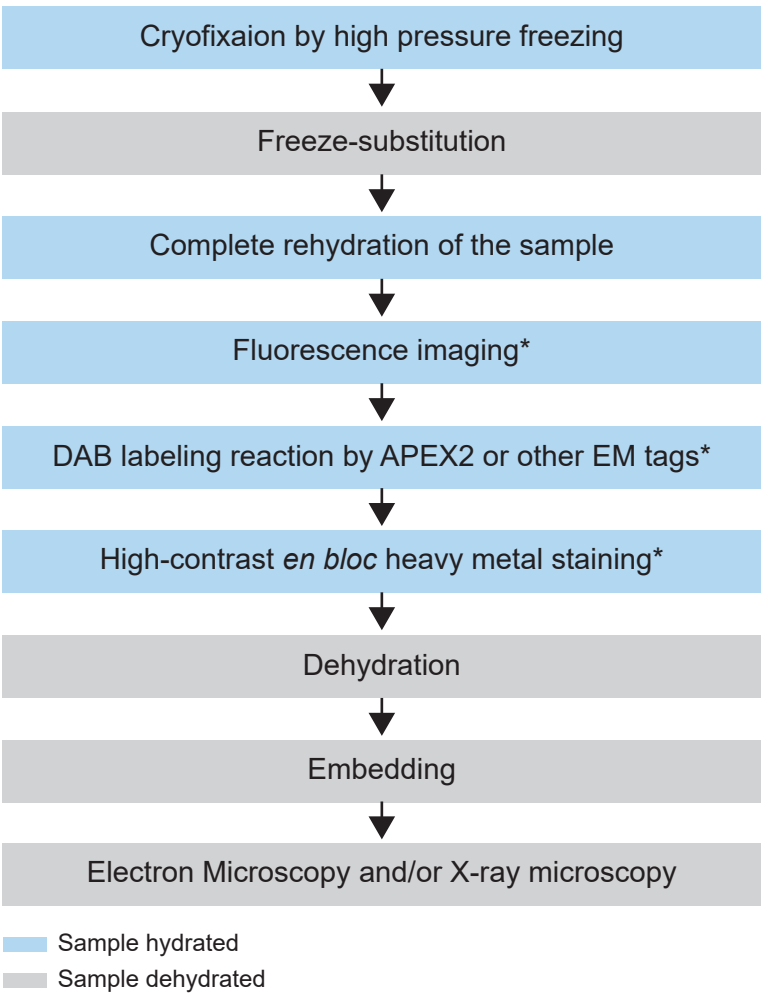

Figure 3

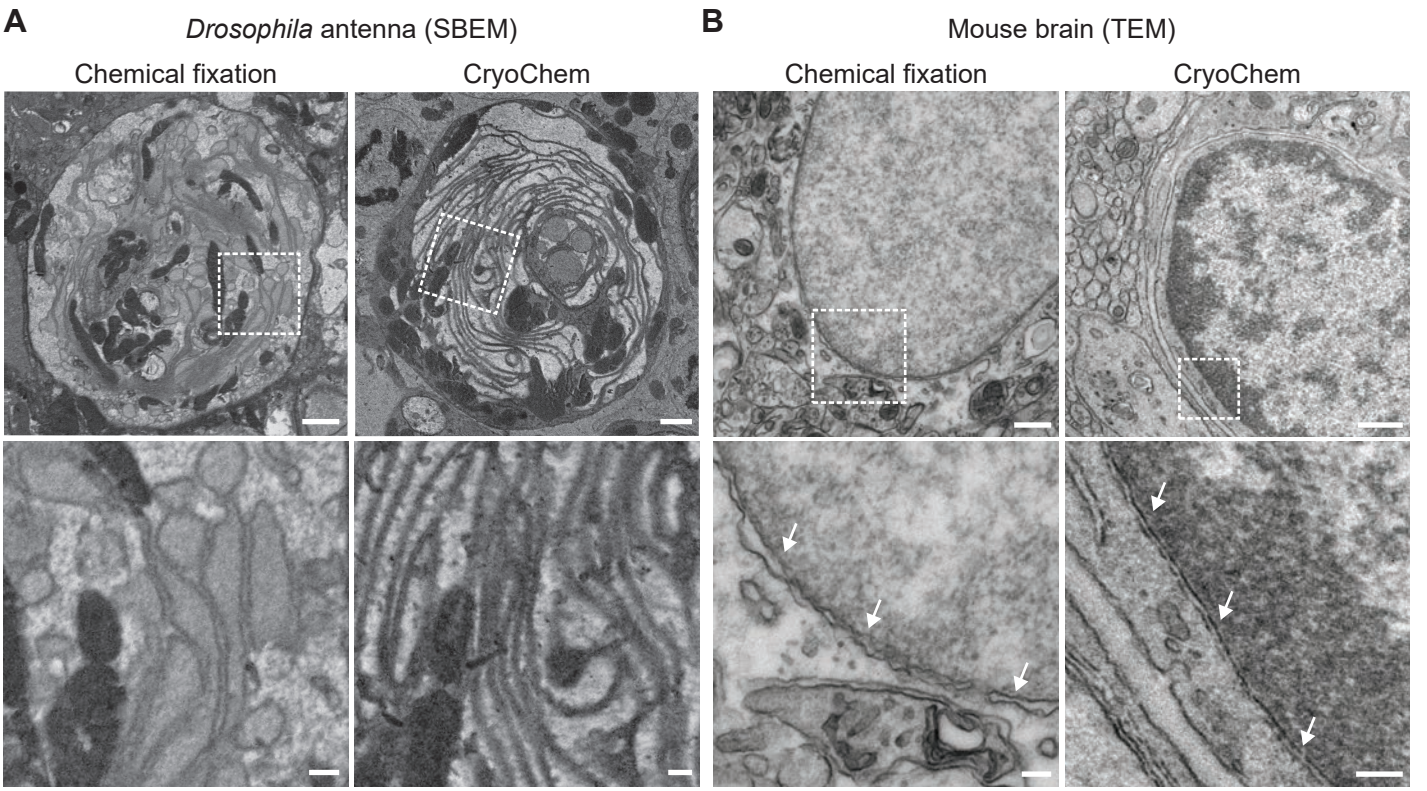

Figure 3-figure supplement 1

Cultured mammalian cells (TEM)

CryoChem

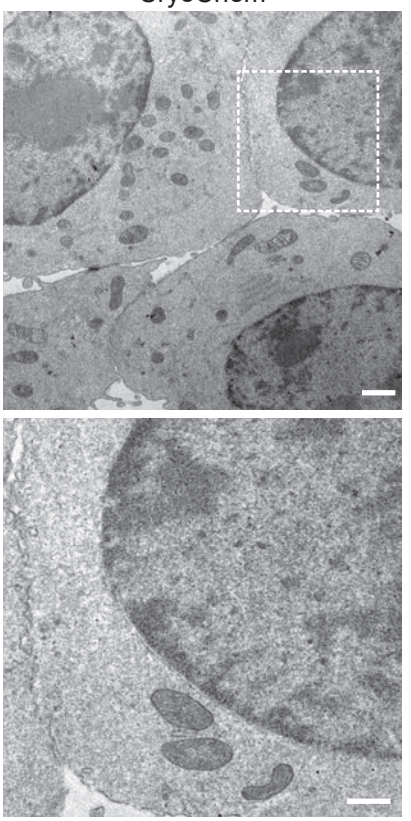

Figure 4

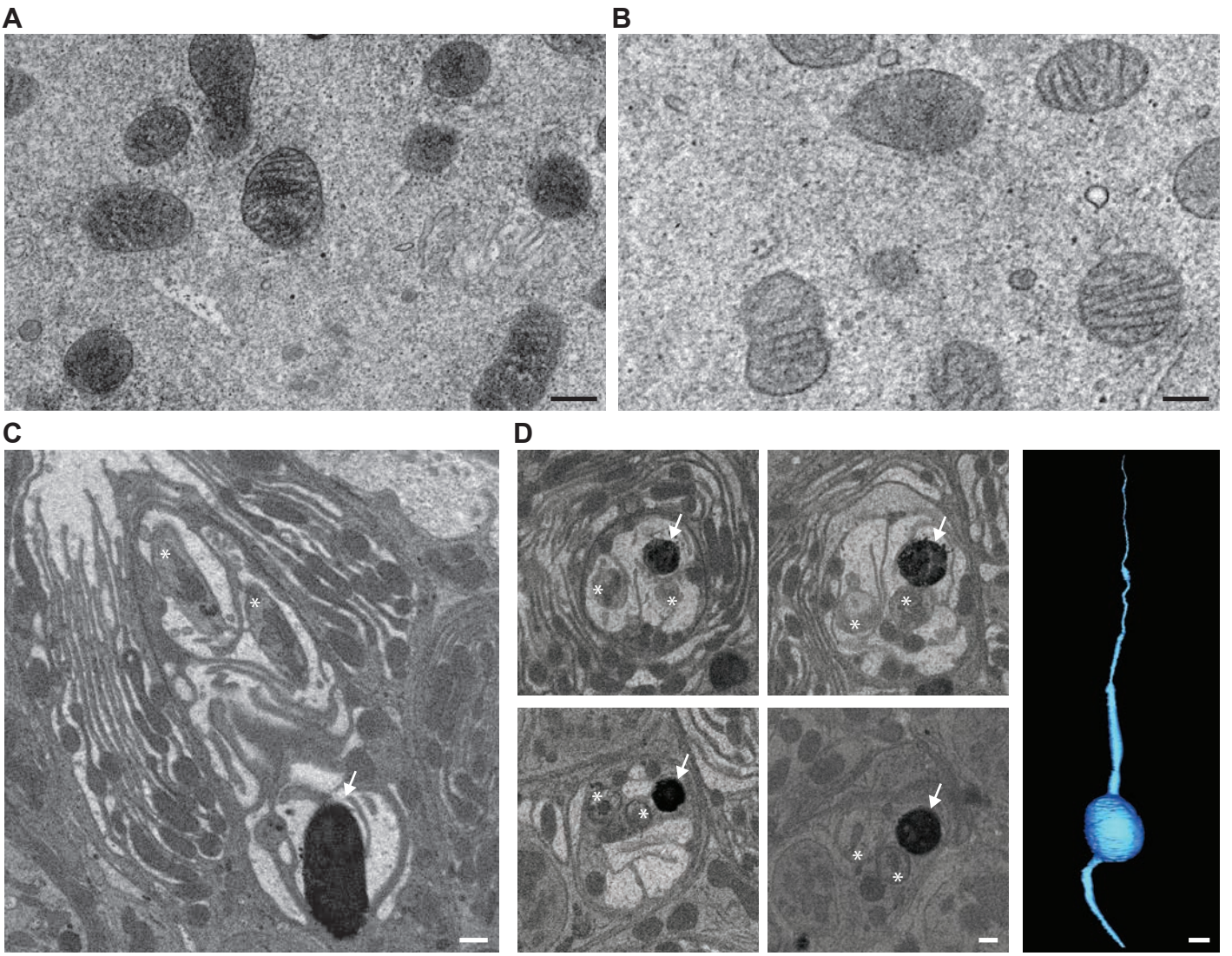

Figure 5

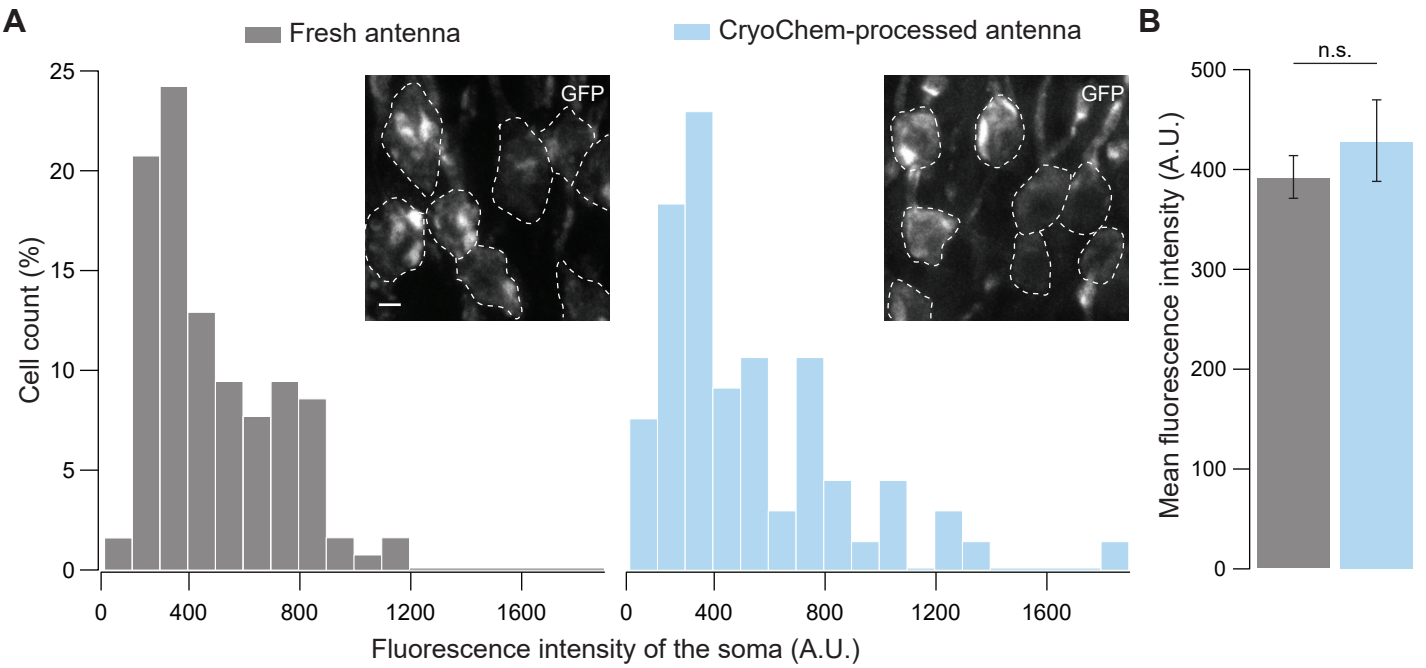

Figure 5-figure supplement 1

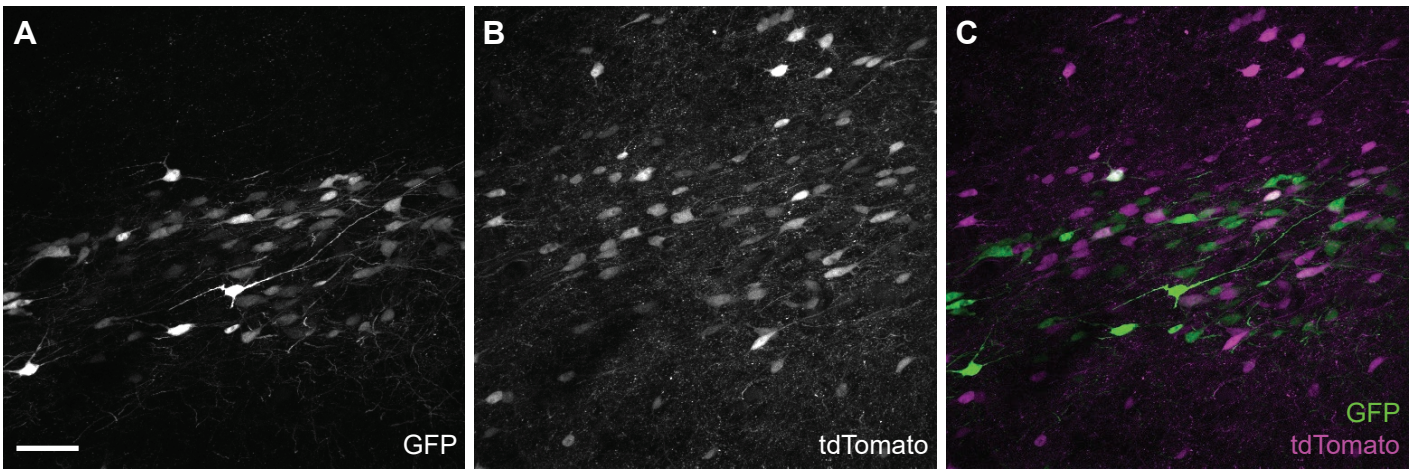

Figure 6